

Determining the Hubble Constant from the Gravitational Lens PG 1115+080

C.R. Keeton

C.S. Kochanek

Harvard-Smithsonian Center for Astrophysics, MS-51
60 Garden Street
Cambridge, MA 02138

ABSTRACT

For the quadruple gravitational lens PG 1115+080, we combine recent measurements of the time delays with new lens models to determine the Hubble constant H_0 . We explore the effects of systematic uncertainties in the lens models on the estimates of H_0 , and we discuss how the uncertainties can be reduced by future observations. We find that the lens cannot be fit by an isolated lens galaxy, but that it can be well fit by including a perturbation from the nearby group of galaxies. To understand the full range of systematic uncertainties it is crucial to use an ellipsoidal galaxy and to let the group position vary. In this case, the existing constraints cannot break degeneracies in the models with respect to the profiles of the galaxy and group and to the position of the group. Combining the known time delays with a range of lens models incorporating most of the plausible systematic effects yields $H_0 = 51^{+14}_{-13}$ km s⁻¹ Mpc⁻¹. The constraints on the lens models, and hence on H_0 , can be improved by reducing the standard errors in the lens galaxy position from 50 mas to ~ 10 mas, reducing the uncertainties in the time delays to ~ 0.5 days, and constraining the lens mass distribution using HST photometry and the fundamental plane. In particular, the time delay ratio $r_{ABC} \equiv \Delta\tau_{AC}/\Delta\tau_{BA}$ may provide the best constraint on the mass profile of the galaxy.

Subject headings: gravitational lensing – cosmology: distance scale – galaxies: structure – quasars: individual (PG 1115+080)

To appear in The Astrophysical Journal

1. Introduction

A general consensus is emerging from local studies that the Hubble constant H_0 lies in the range 65–75 km s⁻¹ Mpc⁻¹ (e.g. Freedman, Madore & Kennicutt 1996), based primarily on Cepheid distances to nearby galaxies combined with type Ia supernovae to reach regions of pure Hubble flow (e.g. Riess, Press & Kirshner 1996). The resulting age estimates are in weak conflict with the estimated ages of the oldest stars for almost all cosmological models (e.g. Bolte & Hogan 1995). Measurements of time delays in gravitational lenses can directly determine H_0 over cosmological distances (Refsdal 1964), thereby avoiding the complicated calibration problems that plague local distance estimates. In a gravitational lens, the ray trajectories of the multiple images have different geometric lengths and pass through different parts of the gravitational potential, so the light travel time is different for each image. The light travel time is inversely proportional to H_0 , so combining observed time delays between images with a model of the gravitational potential gives the Hubble constant. Unfortunately, application of this technique has been slowed by the difficulties of determining the time delays and of finding good models for the gravitational potential.

The first gravitational lens discovered, 0957+561 (Walsh et al. 1979), was also the first lens for which a time delay was measured (e.g. Vanderreist et al. 1992; Lehár et al. 1992; Press, Rybicki & Hewitt 1992a,b; Schild & Thomson 1995; Pelt et al. 1996; Kundić et al. 1996); the most recent measurement yielded the time delay $\Delta\tau = 417 \pm 3$ days at 95% confidence (Kundić et al. 1996). The system has been modeled extensively (e.g. Young et al. 1980; Borgeest & Refsdal 1984; Narasimha, Subramanian & Chitre 1984; Greenfield, Roberts & Burke 1985; Falco, Gorenstein & Shapiro 1991; Kochanek 1991b; Bernstein, Tyson & Kochanek 1993; Grogin & Narayan 1996). Most recently, Grogin and Narayan (1996) considered a spherical softened power-law model for the primary lens galaxy and an external shear for the surrounding cluster. The best-fit galaxy model had a dark matter halo whose mass increases slightly faster than isothermal, $M(r) \propto r^\alpha$ with $1.07 < \alpha < 1.18$ at 95% confidence. This model gave $H_0 = (85_{-7}^{+6}) (1 - \kappa)(\Delta\tau/1.1 \text{ yr})^{-1}$ km s⁻¹ Mpc⁻¹, where $\kappa > 0$ is an inherent degeneracy due to the mean surface mass density of the cluster (Falco, Gorenstein & Shapiro 1985). Kundić et al. (1996) estimated κ from the observation of the cluster by Fischer et al. (1997) and used the model of Grogin & Narayan to infer $H_0 = 64 \pm 13$ km s⁻¹ Mpc⁻¹ (95% confidence); independently, Falco et al. (1997) used the velocity dispersion of the galaxy to infer $H_0 = 62 \pm 7$ km s⁻¹ Mpc⁻¹. We note that Grogin & Narayan (1996) briefly considered an approximate elliptical model of the galaxy, but they fixed the ellipticity and position angle to match the observed isophotes and did not explore the additional freedom in the models (and hence in H_0) due to treating the galaxy and cluster as independent sources of shear.

Recently the four-image gravitational lens PG 1115+080 (Weymann et al. 1980; see Figure 1) became the second lens for which time delays were measured. Schechter et al. (1997) measured the time delay between images C and B to be $\Delta\tau_{BC} = 23.7 \pm 3.4$ days and the time delay between C and mean of the close pair $A = A_1 + A_2$ to be $\Delta\tau_{AC} = 9.4 \pm 3.4$ days, giving a time delay ratio $r_{ABC} \equiv \Delta\tau_{AC}/\Delta\tau_{BA} = 0.7 \pm 0.3$. Bar-Kana (1997), however, reanalyzed the data to show that including the correlations in the photometric errors gives $\Delta\tau_{BC} = 25.0_{-1.7}^{+1.5}$ days and $r_{ABC} = 1.13_{-0.17}^{+0.18}$ (statistical), with a ~ 0.2 systematic uncertainty in r_{ABC} associated with different assumptions about how to treat the photometric errors.

PG 1115+080 is a promising candidate for combining time delays with lens models to determine H_0 , because four-image lens geometries can constrain some aspects of lens models better than two-image lens geometries (Kovner 1987; Kochanek 1991a). PG 1115+080 has been modeled extensively. The first models demonstrated that simple non-axisymmetric galaxy models could qualitatively reproduce the image configuration (Young et al. 1981; Narasimha, Subramanian & Chitre 1982). Further models showed that an isothermal sphere or a point mass with a variety of quadrupole structures could reproduce the image positions to within ground-based observational errors, but that the observations were not accurate enough to distinguish between the various monopole and quadrupole forms (Kochanek 1991a). More accurate observations with the Hubble Space Telescope (Kristian et al. 1993, hereafter K93) have provided better observational constraints. Keeton, Kochanek & Seljak (1997a) showed that the quasar image positions and fluxes and the galaxy position cannot be fit by models with a single shear axis (such as an ellipsoidal galaxy or a circular galaxy with an external shear), but can be fit by models allowing two independent shear axes (such as an ellipsoidal galaxy with an external shear). Schechter et al. (1997) demonstrated that the nearby group of galaxies seen by Young et al. (1981) can provide the required external shear. In addition, Schechter et al. (1997) used their measurements of the time delay with a simple lens model treating the galaxy and group as singular isothermal spheres to infer $H_0 = 42 \text{ km s}^{-1} \text{ Mpc}^{-1}$, with a 14% uncertainty from the time delay and with unknown uncertainties from the lens model. Their value for H_0 is in strong conflict with local estimates of $H_0 = 65\text{--}75 \text{ km s}^{-1} \text{ Mpc}^{-1}$, so it is crucial to understand the systematic uncertainties in the lens models and their effects on the inferred value of H_0 . In addition, if we hope to use lensing to measure H_0 with precision comparable to the distance ladder, then we must understand which future observations can reduce the uncertainties in the lens models.

In this paper we examine the systematic uncertainties in the value of H_0 inferred from PG 1115+080 by exploring the uncertainties in the lens models. Since present observations of the galaxy and group do not directly constrain their mass distributions and only weakly constrain their positions, we postulate a wide range of plausible galaxy

and group properties. Specifically, we model the galaxy as an ellipsoidal mass distribution with a range of profiles including constant mass-to-light ratio models, standard dark matter models, and more centrally-concentrated models. We model the group as a circular mass distribution with an extended (isothermal) or concentrated (point mass) profile. We then study the ability of the data to constrain the models and show that present constraints leave significant degeneracies in the models. We examine the implications of the models and degeneracies for H_0 , and discuss future observations that can break the degeneracies and improve the constraints on H_0 . In §2 we present the data and methods used in the models. In §3 we consider a broad range of models using only the primary lens galaxy and show that they cannot fit the data. In §4 we study models adding the nearby group and show that a variety of galaxy+group models give good fits. We use a Bayesian analysis with the most physically plausible models to quantify the present systematic uncertainties in H_0 . In §5 we illustrate an independent way to break one degeneracy by using stellar dynamics and the fundamental plane of elliptical galaxies to identify which galaxy profiles are physically plausible. In §6 we summarize our results for H_0 as well as the prospects for breaking the degeneracies through better observations of the quasar fluxes, the galaxy position and photometry, and the time delays.

2. Data and Methods

PG 1115+080 consists of four point images of a $z_s = 1.722$ quasar with separations $\sim 2''$ surrounding a galaxy at redshift 0.295 ± 0.005 (Weymann et al. 1980; K93; Angonin-Willaime et al. 1993). There is a nearby group of galaxies (Young et al. 1981) at redshift 0.304 (Henry & Heasley 1986). A schematic diagram of the lens and the galaxies is shown in Figure 1. For reference, in an $\Omega_0 = 1$ cosmology $1''$ at the group redshift is $2.77h^{-1}$ kpc. Other cosmological scale factors used in the lensing analysis are given in Table 1 for several cosmologies. Throughout the text we use an $\Omega_0 = 1$ cosmology.

Computing H_0 from a gravitational lens requires time delays and a lens model. The time delays were taken from Bar-Kana’s (1997) analysis of the data of Schechter et al. (1997). The $B - C$ time delay is the longest and best-resolved time delay. Bar-Kana (1997) found $\Delta\tau_{BC} = 25.0^{+1.5}_{-1.7}$ days, consistent with the value 23.7 ± 3.4 days from Schechter et al. (1997), and this result depended only weakly on assumptions about the photometric errors. By contrast, the other time delays and hence the time delay ratio $r_{ABC} \equiv \Delta\tau_{AC}/\Delta\tau_{BA}$ are less well determined. Bar-Kana (1997) found $r_{ABC} = 1.13^{+0.18}_{-0.17}$, in conflict with the value 0.7 ± 0.3 from Schechter et al. (1997), and this result did depend on assumptions about the photometric errors. A range of assumptions indicated that Bar-Kana’s (1997) result

for r_{ABC} was more robust than the result of Schechter et al. (1997), and that systematic uncertainties in r_{ABC} were at the level of ~ 0.2 (Bar-Kana 1997).

To determine the lens model, we fitted lens mass distributions to reproduce the quasar images positions and fluxes and the galaxy position from the Hubble Space Telescope observations by K93 (see Table 2). The relative coordinates have an uncertainty of 5 mas for the quasar images and 50 mas for the lens galaxy. The quasar flux ratios are less well determined because of the source variability, microlensing, and extinction. To account for this, we broadened the flux error bars to 20% to encompass the range of observed variability (see Keeton & Kochanek (1996) for a summary). We also considered the effects on our conclusions of making the flux error bars smaller (see §6). K93 estimated the upper limit on the flux of a faint central image to be 1–2% of the flux of the brightest image, and we included this constraint by setting the limit on the flux of the central image to be $0 \pm 2\%$ of the flux of the brightest image.

Time delays offer an independent constraint on lens models, but only if more than one is known. The first time delay is used to determine H_0 , and the rest are combined into H_0 -independent ratios that constrain the models. However, because of the systematic uncertainties in the time delays for PG 1115+080 we used them only to determine H_0 , not to constrain the models. For each model, we used the $B - C$ time delay to compute H_0 , which we express as $H_0 = 100h_{BC}(\Delta\tau_{BC}/25.0 \text{ days})^{-1} \text{ km s}^{-1} \text{ Mpc}^{-1}$. We used the other known time delay in the ratio r_{ABC} only as a qualitative check of the consistency of the models. We did, though, examine the effects of including the r_{ABC} constraint in the Bayesian analysis of H_0 in §4.2.

To determine whether a lens mass distribution is consistent with the data, we studied the images it can produce. The lensing properties of a surface mass distribution Σ are described by its lensing potential ψ determined from the two-dimensional Poisson equation $\nabla^2\psi = 2\Sigma/\Sigma_{cr}$ (e.g. Schneider, Ehlers & Falco 1992), where the critical surface density for lensing in angular units is

$$\Sigma_{cr} = \frac{c^2}{4\pi G} \frac{D_l D_s}{D_{ls}} = 2.34h^{-1} \left[\frac{D_l D_s}{2r_H D_{ls}} \right] \times 10^{11} M_\odot \text{ arcsec}^{-2}, \quad (1)$$

$r_H = c/H_0$ is the Hubble radius, and D_l , D_s , and D_{ls} are angular diameter distances to the lens, to the source, and between the lens and the source, respectively. Values of the distance ratio are given in Table 1. The potential ψ describes the mapping between the source and image planes through the lens equation

$$\vec{u} = \vec{x} - \vec{\nabla}\psi(\vec{x}), \quad (2)$$

where \vec{x} is an angular position in the image plane and \vec{u} is an angular position in the source plane. A source at \vec{u} maps to images at \vec{x}_i that are roots of the lens equation. The

images are deformed by the magnification tensor M_{ij} where $M_{ij}^{-1} = \delta_{ij} - \partial^2\psi/\partial x_i\partial x_j$. Because surface brightness is conserved, the total magnification of an image is the ratio of the area of the magnified image to the area of the source; so the magnification factor is $M = \det(M_{ij})$. The ray trajectories of the images have different geometric lengths and pass through different parts of the gravitational potential, so the light travel time is different for each image; the time at image position \vec{x} is

$$\tau(\vec{x}) = \frac{1+z_l}{c} \frac{D_l D_s}{D_{ls}} \left[\frac{1}{2} (\vec{x} - \vec{u})^2 - \psi(\vec{x}) \right], \quad (3)$$

and the time delay between an image at \vec{x}_i and an image at \vec{x}_j is $\Delta\tau_{ij} = \tau(\vec{x}_i) - \tau(\vec{x}_j)$. Note that τ factors into a piece that depends on the lens model times a piece that depends on cosmology and scales as H_0^{-1} (see Table 1 for values in different cosmologies). If we let $\tilde{D} = D/r_H$ be an angular diameter distance scaled by r_H (and hence independent of H_0), then we can use eq. (3) to find H_0 from a lens model and time delay,

$$H_0 = \frac{1+z_l}{\Delta\tau_{ij}} \frac{\tilde{D}_l \tilde{D}_s}{\tilde{D}_{ls}} \left[\frac{1}{2} (|\vec{x}_i - \vec{u}|^2 - |\vec{x}_j - \vec{u}|^2) - (\psi(\vec{x}_i) - \psi(\vec{x}_j)) \right]. \quad (4)$$

From Table 1, changing the cosmology can change the inferred value of H_0 by up to 7%.

We modeled the primary lens galaxy with ellipsoidal surface mass densities of the form

$$\Sigma = \Sigma(m^2) \quad \text{where} \quad m^2 = r^2 \left(1 + \epsilon \cos 2(\theta - \theta_\epsilon) \right), \quad (5)$$

ϵ is a natural ellipticity parameter such that the axis ratio is $(1 - \epsilon)^{1/2}/(1 + \epsilon)^{1/2}$, and θ_ϵ is the orientation angle of the major axis. We will quote θ_ϵ as a standard position angle measured North through East. We considered two classes of models. First, we used the de Vaucouleurs (1948) model as the prototypical constant mass-to-light ratio (M/L) model for early-type galaxies, with surface mass density

$$2 \frac{\Sigma}{\Sigma_{cr}} = \frac{b}{r_e} \frac{\exp \left\{ -k (m^2/r_e^2)^{1/8} \right\}}{\int_0^\infty dv v \exp \left\{ -k v^{1/4} \right\}}, \quad (6)$$

where $k = 7.67$, r_e is the effective (or half-light) radius, and b is the deflection scale such that the total mass is

$$M_{tot} = \frac{b r_e}{\sqrt{1 - \epsilon^2}} \frac{c^2}{4G} \frac{D_l D_s}{D_{ls}} = 7.36 h^{-1} \frac{b r_e}{\sqrt{1 - \epsilon^2}} \left[\frac{D_l D_s}{2 r_H D_{ls}} \right] \times 10^{11} M_\odot \quad (7)$$

for b and r_e in arcseconds. Second, we used softened power-law models with surface mass density

$$2 \frac{\Sigma}{\Sigma_{cr}} = \frac{b^{2-\alpha}}{(s^2 + m^2)^{1-\alpha/2}}, \quad (8)$$

where α is the power law exponent such that $M(r) \propto r^\alpha$ asymptotically, s is a core radius, and b is the deflection scale. For $\alpha = 1$ it is a softened isothermal model, whose lensing properties have been studied by Kassiola and Kovner (1993) and Kormann, Schneider & Bartelmann (1994). For $\alpha = 0$ it is a modified Hubble model (Binney & Tremaine 1987). We also studied the more centrally-concentrated $\alpha = -1$ model. For $\alpha = 1, 0, -1$ we found analytic expressions for the deflection and the magnification, and for other values of α we used numerical integrals.

We modeled the group as a single halo in which the observed galaxies are embedded. For simplicity we used only circular mass distributions. We considered a standard dark matter model treating the group as a singular isothermal sphere (SIS), and we studied the effects of making it more centrally concentrated by considering the limit of a point mass. The lensing potential for a point mass at the origin is $\psi(r) = b^2 \ln r$.

For a given lens mass distribution, we solved the lens equation (2) to map a source at \vec{u} to its images at \vec{x}_i . We varied the position and flux of the source and the parameters of the mass distribution using the “amoeba” downhill simplex method (Press et al. 1992) to minimize the residuals in the image plane. We included in the χ^2 the constraints from the quasar positions and fluxes and the galaxy position. The galaxy position and the four quasar positions and fluxes provide 14 constraints. A galaxy model with r_e or (s, α) fixed has five free parameters (\vec{x}_{gal} , ϵ , θ_ϵ , and b). A group model has one parameter (b_{grp}) if the position is fixed and three parameters if the position is variable. The source has three parameters (\vec{u} and the flux). Thus a lens model using an isolated lens galaxy with fixed r_e or (s, α) has $N_{dof} = 6$ and a lens model using the galaxy plus a movable group has $N_{dof} = 3$.

3. Results: Isolated Galaxy

We first considered simple lens models using only the primary lens galaxy. Previous studies showed that the K93 data cannot be fitted by an isolated lens galaxy if the galaxy is represented by a point mass or a singular isothermal mass distribution (Keeton et al. 1997; Schechter et al. 1997). To see whether some other isolated galaxy could fit the data, we considered a range of softened power-law models, as well as de Vaucouleurs constant M/L models. For all models we used an ellipsoidal mass distribution as the source of shear.

For the de Vaucouleurs models, there are no observational estimates of the effective radius r_e , so we tabulated results as a function of r_e (see Figure 2). To estimate the plausible range of r_e , we note that an L_* galaxy has an effective radius of $(4 \pm 1)h^{-1}$ kpc (Kormendy & Djorgovski 1989; Rix 1991), which corresponds to $1''.4$ at the redshift of

PG 1115+080. In addition, in §5 we use stellar dynamical arguments to estimate that r_e lies in the range $1''.0 \lesssim r_e \lesssim 4''.0$. With this range of effective radii, no de Vaucouleurs model gives an acceptable fit. The χ^2/N_{dof} is 68 at $r_e = 1''.5$ ($4.2h^{-1}$ kpc) and is even larger at smaller effective radii. Although χ^2/N_{dof} decreases for larger r_e , it is still 18 at $r_e = 10''$ ($28h^{-1}$ kpc). All physical parameters inferred from the models are unreasonable: for $r_e = 0''.5\text{--}4''.0$, the models require a very flattened galaxy ($b/a \sim 0.1\text{--}0.4$) and imply a huge Hubble constant ($h_{BC} \sim 2.3\text{--}1.3$). Moreover, the ratio of the model $A_1 - C$ and $B - A_1$ time delays is $r_{ABC} \sim 5.4\text{--}2.0$, compared with 0.7 ± 0.3 for the time delays of Schechter et al. (1997) or 1.13 ± 0.2 for the time delays of Bar-Kana (1997). A simple constant M/L galaxy cannot describe PG 1115+080.

For the softened power-law models, we tabulated the results in the plane of the core radius s and the power-law exponent α (see Figure 2). Generally the softened power-law profiles fit much better than the de Vaucouleurs profile but still do not give a good fit. The best-fit model has $\chi^2/N_{dof} = 11.7$, is nearly isothermal ($\alpha = 1.002$), and has a large core radius ($s = 0''.45 = 1.2h^{-1}$ kpc). This model implies an axis ratio $b/a = 0.75$, a Hubble constant $h_{BC} = 0.50$, and a time delay ratio $r_{ABC} = 1.44$ that is marginally consistent with Bar-Kana (1997) given his systematic uncertainties. As s or α decreases, the models become more centrally-concentrated and imply larger values for H_0 ; this is because H_0 scales as $1 - \kappa_0$ where κ_0 is the convergence at the critical radius (Falco et al. 1985), and the models with steeper profiles have a smaller κ_0 . The models are not tightly constrained, with the 1σ region allowing core radii $0''.28$ ($0.8h^{-1}$ kpc) $\lesssim s \lesssim 0''.55$ ($1.5h^{-1}$ kpc), and power-law exponents $0.7 \lesssim \alpha \lesssim 1.6$. Profiles steeper than the modified Hubble profile ($\alpha = 0$) are ruled out at better than 99.9% confidence. Over the 1σ region, r_{ABC} is well constrained and varies by only ~ 0.1 , but h_{BC} is poorly constrained and varies from 0.2 to 0.7. For reference, the singular isothermal ellipsoid model has $\chi^2/N_{dof} = 25$, $b/a = 0.50$, $h_{BC} = 0.94$, and $r_{ABC} = 1.85$.

It is surprising that the models require such a large core radius even for the isothermal profile. We expect a small core radius for two reasons. First, observations of galactic cores show that the luminosity densities of elliptical galaxies do not have flat cores but instead have central cusps (Gebhardt et al. 1996). Second, it is generally argued that small core radii are needed to fit lens data, both because almost all known lenses lack a central image, and because stellar dynamics, lens statistics, and other lens models are consistent with isothermal mass distributions with small core radii (Narasimha, Subramanian & Chitre 1986; Kassiola & Kovner 1993; Wallington & Narayan 1993; Kochanek 1993, 1995, 1996; Grogin & Narayan 1996). Contrary to these expectations, PG 1115+080 cannot be fit by an isolated lens galaxy with a small core radius. It is difficult, though, to draw strong conclusions from this result because the “best-fit” model is still not a good fit

($\chi^2/N_{dof} = 11.7$), while once we include the perturbation from the group we will find good fits ($\chi^2/N_{dof} \lesssim 1$) with galaxies that do have a small core radius.

We conclude that PG 1115+080 cannot be fit by an isolated lens galaxy, and thus it is not reasonable to use such a model to estimate H_0 .

4. Results: Galaxy + Group

Keeton et al. (1997a) found that while PG 1115+080 could not be fit by an isolated isothermal galaxy, it could be well fit by an ellipsoidal galaxy with an independent external shear. Schechter et al. (1997) pointed out that the group seen by Young et al. (1981) was correctly located to be the source of the shear, and by modeling the galaxy and the group as two singular isothermal spheres they inferred $H_0 = 42 \text{ km s}^{-1} \text{ Mpc}^{-1}$. This value of H_0 is unexpectedly low, but it is difficult to judge its significance because Schechter et al. (1997) did not explore the systematic uncertainties in the lens models and their effects on the inferred H_0 . In order to understand the systematic effects, we now examine the galaxy+group models in detail. We explore the freedom in the models (and hence in H_0) and discuss the prospects for better constraining the models with future observations. First we consider models with the group position fixed to examine the effects of the profiles of the galaxy and the group, and then we consider models in which the group position is allowed to vary.

4.1. Fixed group

The group mass distribution is described by a position and any parameters associated with the radial profile. Let d_{grp} be the distance from the primary lens galaxy to the group, and b_{grp} be the critical radius of the group. To lowest order the group is a perturbation that can be characterized by its convergence κ_{grp} and shear γ_{grp} together with weaker nonlinear terms (Falco et al. 1985). For a singular isothermal sphere (SIS) group $\gamma_{grp} = \kappa_{grp} = b_{grp}/2d_{grp}$, while for a point mass group $\gamma_{grp} = b_{grp}^2/d_{grp}^2$ and $\kappa_{grp} = 0$. Since γ_{grp} scales with b_{grp}/d_{grp} , we expect that requiring an external shear $\gamma_{grp} \sim 10\%$ (Kochanek 1991a; Keeton et al. 1997a; Schechter et al. 1997) will produce (to lowest order) a degeneracy between the group’s position and its mass. The non-linear terms may break the degeneracy (see §4.2), but for simplicity we first consider models with the group position fixed. In this way we can focus on the effects of different profiles for the galaxy and the group.

The three group galaxies and the lens galaxy are at essentially the same redshift and are probably physically related, so we placed the group at the flux-weighted centroid of all four galaxies (C4 in Figure 1). The Gunn r magnitudes of the three group galaxies were taken from Young et al. (1981); the r magnitude of the primary lens galaxy was estimated from the F785LP magnitude (K93) by using the galaxy evolution models of Bruzual & Charlot (1993) to compute the color of an E/S0 galaxy at a redshift of 0.3 (see Keeton, Kochanek & Falco 1997b for details). We found the flux centroid to be $d_{grp} = 14''.5$ from the primary lens galaxy at a position angle $\theta_{grp} = -117^\circ.1$ (North through East).

Figure 3 shows the results for de Vaucouleurs, softened isothermal ($\alpha = 1$), modified Hubble ($\alpha = 0$), and $\alpha = -1$ models of the primary lens galaxy with either an SIS or a point mass group, and Table 3 summarizes the χ^2 and the physical parameters for the best fits. All eight classes of models give good fits, with $\chi^2/N_{dof} < 1$ for all but the model with an $\alpha = -1$ galaxy and a point mass group. Since no model with an isolated galaxy could do better than $\chi^2/N_{dof} \sim 10$, while numerous models with the galaxy supplemented by the group produce $\chi^2/N_{dof} \lesssim 1$, we confirm the results of Keeton et al. (1997a) and Schechter et al. (1997) that including the group is crucial to obtaining a good fit. We note that the best model of Schechter et al. (1997), which treated the galaxy and group and singular isothermal spheres, gave $\chi^2/N_{dof} = 5$. Our models give $\chi^2/N_{dof} < 1$ despite the addition of the flux constraints because we allowed the galaxy position to vary, and because we included a second shear by allowing the galaxy to have an ellipticity. As we noted in Keeton et al. (1997a), the key to fitting many of the quadruple lenses is having two independent shear axes.

The values for h_{BC} implied by these models vary significantly with the galaxy and group profiles (see Table 3). Qualitatively, the variation makes sense: H_0 scales with $1 - \kappa_0$ (Falco et al. 1985), and the convergence κ_0 at the critical radius decreases as the galaxy or group becomes centrally concentrated. Unfortunately, the data cannot constrain the profiles for two reasons. First, although the four-image configuration constrains the total mass within the critical radius, it does not constrain the distribution of the mass (Kochanek 1991a; Wambsganss & Paczyński 1994). Second, although the quasar images constrain the shear from the group, they do not constrain its mass or convergence. As a result, we can have a wide range of galaxy and group profiles that are all consistent at the 1σ level, and by using different profiles we can produce h_{BC} anywhere from 0.4 to more than 0.8 without significantly changing the goodness of fit. As we show in §5, though, not all of the profiles corresponds to galaxies that are physically plausible. The centrally concentrated models that allow the higher values for H_0 correspond to galaxies that do not lie on the fundamental plane of elliptical galaxies. Restricting attention to plausible dark matter and constant M/L models restricts the range of h_{BC} to $0.4 \lesssim h_{BC} \lesssim 0.7$.

4.2. Movable group

While fixing the group at the flux centroid C4 allowed us to isolate the effects of the profiles of the galaxy and group, there is no strong observational evidence requiring it. Hence the group position is an additional systematic uncertainty whose effects on H_0 must be examined. We studied the effects of the group position for two galaxy models: a dark matter (isothermal) model and a constant M/L model. For the constant M/L model we used a modified Hubble profile because, although it is not as good a representation of galaxy luminosity profiles as the de Vaucouleurs profile, it does have an analytic deflection formula. We neglected the more centrally concentrated galaxy models because, as we show in §5, they require galaxies that are unphysical. For the group we again used the SIS and point mass models. Physically we expect the group to be described by an isothermal dark matter halo, but by including the point mass group we can examine the effects of making the group more concentrated. Since these two galaxy profiles and two group profiles span the expected range of mass profiles, they should span the expected range of H_0 . We examined all four combinations of profiles; representative results are shown in Figures 4 and 5, where Figure 4 shows the extended profiles (isothermal galaxy and SIS group), and Figure 5 shows the concentrated profiles (modified Hubble galaxy and point mass group).

The singular isothermal ellipsoid (dark matter) galaxy permits good fits for a wide range of group positions (see Figure 4). With an SIS group, the best-fit model is at $d_{grp} = 25''.2$ and $\theta_{grp} = -125^\circ$, has $\chi^2 = 1.77$ for $N_{dof} = 3$, and implies $h_{BC} = 0.47$. But at the 1σ level, θ_{grp} can range from -150° to -110° and d_{grp} can be as small as a few arcseconds. The Hubble constant varies considerably over the allowed region, from $h_{BC} = 0.2$ for distant groups with $\theta_{grp} \simeq -113^\circ$, to $h_{BC} = 0.7$ for nearby groups or for distant groups with $\theta_{grp} \simeq -145^\circ$.

Note that there is no formal upper limit on d_{grp} from the χ^2 , because for a distant group the non-linear terms are weak and the perturbation is equivalent to a simple external shear, which we know fits well (Keeton et al. 1997a). However, the mass of the group increases with its distance ($M_{grp} \propto b_{grp} d_{grp} \sim d_{grp}^2$), so requiring that the group have a reasonable mass can constrain its position. It is convenient to study the mass of the group in terms of its mass-to-light ratio (M/L), and it is convenient to express the M/L of the group in units of the M/L of the galaxy because this ratio is independent of assumptions about the cosmology and about the K and evolutionary corrections to the luminosities. The models with the group in a band from the centroid C4 to the best-fit group position have $5 \lesssim (M/L)_{grp}/(M/L)_{gal} \lesssim 25$. The galaxy mass within the critical radius (radius $r_0 = 1''.14 = 3.16h^{-1}$ kpc) is $1.22 \times 10^{11}h^{-1} M_\odot$, with a 5% uncertainty due to the position of the group, a 10% uncertainty (upwards) due to making the group

more centrally concentrated, and a 7% uncertainty (upwards) due to the cosmological model. Using the K93 F785LP central aperture magnitude together with color, K , and evolutionary corrections from the galaxy evolution models of Bruzual & Charlot (1993), we estimated the present B magnitude of the galaxy to be -19.2 mag for an $\Omega_0 = 1$ cosmology (see Keeton et al. 1997b for details), although the effective aperture of the K93 magnitude is unclear. This gives $(M/L)_{gal} \simeq 18$, which is consistent with other lens models (Keeton et al. 1997b) and lens statistics (Kochanek 1993, 1996; Maoz & Rix 1993). This in turn implies $90 \lesssim (M/L)_{grp} \lesssim 450$, which is consistent with observed group mass-to-light ratios, e.g. $150 \lesssim M/L \lesssim 350$ (Ramella, Pisani & Geller 1997). It is difficult at present to apply strong constraints from this reasoning, but it is clear that the group positions that give good fits also give reasonable group masses and that the group should not be much closer or much farther away.

Figure 4 shows that at present the constraints on H_0 are relatively weak. Nevertheless, the models imply several physical properties that may be better constrained by future observations. First, the galaxy positions differ at the level of tens of mas. While the K93 position is well within the range of good fits, the 50 mas error bars are too broad to rule out many models. Reducing the error bars on the galaxy position to 10 mas or better would greatly improve the constraints on the models. Second, the galaxy axis ratios vary. The galaxy is strictly circular if the group is at $d_{grp} = 13''.5$, $\theta_{grp} = -115^\circ$ (which reproduces the double SIS model of Schechter et al. 1997). For other group positions the galaxy’s ellipticity and orientation adjust so the combined shear from the galaxy and group gives a good fit. The ellipticity needs to vary by only a few times 0.05 in order to produce good fits for a wide variety of group positions. Finally, the time delays vary. Although it was not included as a constraint, the ratio r_{ABC} is marginally consistent with the value 1.13 ± 0.2 of Bar-Kana (1997) given his systematic uncertainties of ~ 0.2 . Note that no models produce a time delay ratio consistent with the value $r_{ABC} = 0.7 \pm 0.3$ of Schechter et al. (1997). The time delay ratio could provide a strong constraint on the models if the systematic effects in the observed ratio were understood and if the uncertainties were reduced to ~ 0.05 . This would require roughly a factor of four reduction in the uncertainties in the time delays, or uncertainties of $\lesssim 0.5$ days. We note also that the variation of the $A_2 - A_1$ time delay with group position differs from that of the $A - C$ and $B - A$ time delays, so this time delay could provide an independent constraint. However, $\Delta\tau_{A_2A_1} = 5 \pm 1$ hours over the 1σ region so this time delay would need to be known at the level of ~ 0.5 hour in order to constrain the models.

The results are similar for the modified Hubble model (constant M/L) galaxy, except that good fits are limited to a narrower range of group positions (see Figure 5). With a fixed core radius $s = 0''.2$ ($0.55h^{-1}$ kpc) and a point mass group, the best-fit model is at

$d_{grp} = 28''.3$ and $\theta_{grp} = -118^\circ$, has $\chi^2 = 1.70$ for $N_{dof} = 3$, and implies $h_{BC} = 0.67$. At the 1σ level, θ_{grp} is restricted to $-120^\circ \lesssim \theta_{grp} \lesssim -112^\circ$ and the group can be no closer than $d_{grp} = 11''$. As with the isothermal galaxy, the Hubble constant varies considerably over the 1σ region, ranging from 0.3 to 0.9. However, again physical parameters including the galaxy position, the galaxy axis ratio, and the time delays may be constrained by further observations to improve the constraints on H_0 . In particular, note that the modified Hubble galaxy predicts a time delay ratio that is closer to the observed value of Bar-Kana (1997) than the ratio predicted by the isothermal galaxy. Although it is not shown, the predicted time delay ratio is essentially independent of the profile of the group. Thus if Bar-Kana’s (1997) value remains valid as its uncertainties are reduced, then it may provide the strongest probe of the galaxy profile. We will return to this point below.

Given the wide range of group positions that provide good fits, it is difficult to use the χ^2 statistic to place limits on H_0 . We can, however, use a Bayesian analysis to give a reasonable estimate of the systematic uncertainties. Using Bayes’s theorem we can convert the probability of the data given the parameters (given by $e^{-\chi^2/2}$) into the probability of the parameters given the data. We can then compute the probability distribution for H_0 by integrating over the group position, weighted by a “prior” probability distribution which we took to be a circular Gaussian distribution centered on the flux centroid C4 with standard deviation given by the rms distance of the four galaxies from the centroid. This is roughly the same as the range of group positions permitted by the group mass-to-light ratio. With the probability distribution for H_0 we can characterize the systematic uncertainties in H_0 due to the group position, and also estimate the relative likelihoods of the four classes of galaxy/group profiles. In addition, because the four classes of profiles span the range of physically plausible models (a dark matter or constant M/L galaxy, and an extended or concentrated group), we can combine them to produce a “total” probability distribution that includes the systematic effects of both the group position and the galaxy/group profiles. Figure 6 shows the normalized probability distributions and inferred values of H_0 for the four classes of models, together with the total probability distribution. Since the time delay ratio r_{ABC} may provide a strong constraint on the galaxy profile but is still relatively uncertain, we have computed the probability distributions with and without the formal r_{ABC} constraint from Bar-Kana (1997).

The Bayesian analysis emphasizes two important features of the uncertainties in H_0 due to systematic uncertainties in the lens models. First, using two independent shears (an ellipsoidal galaxy and a movable group) strongly affects H_0 . Dark matter models that have only a single variable shear, such as the models of Schechter et al. (1997) with a circular galaxy or the models of §4.1 with the group position fixed, give $H_0 \simeq 40 \text{ km s}^{-1} \text{ Mpc}^{-1}$. By contrast, dark matter models with two shears give $H_0 = 58_{-15}^{+12} \text{ km s}^{-1} \text{ Mpc}^{-1}$. Thus to

understand the systematic uncertainties in H_0 it is important to consider models with two independent shears. Moreover, since lens models that require two independent shears often have a degeneracy between the shears (Keeton et al. 1997a), such models will generically produce large uncertainties in H_0 that can be reduced only by improving the constraints on the models.

Second, the time delay ratio r_{ABC} is an important constraint on the profile of the galaxy. The current estimate reduces the range of models that are consistent with the data (especially the models that predict large H_0), and reduces the probability of the isothermal galaxy compared with the Hubble galaxy. Without the r_{ABC} constraint, the isothermal galaxy is more likely than the Hubble galaxy by a ratio of 4 : 1, largely because the isothermal galaxy allows such a wide range of group positions. By contrast, with the r_{ABC} constraint the Hubble galaxy increases in likelihood because it produces values for r_{ABC} that are more consistent with Bar-Kana’s (1997) value. Reducing the uncertainties in r_{ABC} thus should help discriminate between the dark matter and constant M/L galaxy models and provide the best probe of the galaxy profile. Using the formal r_{ABC} constraint from Bar-Kana’s (1997) present estimate, the total probability distribution gives $H_0 = 51^{+14}_{-13}$ km s⁻¹ Mpc⁻¹, where these error bars incorporate most of the systematic uncertainties in the lens models due to the group position and the galaxy/group profiles.

5. Stellar Dynamics

To this point we have evaluated models purely on their ability to fit the gravitational lens data, and we have found that the data leave significant degeneracies in the models. One degeneracy is related to the galaxy profile, but here we can apply independent constraints to try to break the degeneracy. Specifically, we can consider whether the galaxies required to fit the lensing data are consistent with stellar dynamics. For example, we suspect that the centrally concentrated models—the models that allow high values for H_0 —may be unphysical.

The absence of information on the optical structure of the lens galaxy limits the conclusions that can be drawn from stellar dynamical models because such models require the luminosity distribution to estimate the stellar velocities. We assume that the galaxy is an early-type galaxy because of its high mass and the expected dominance of lens statistics by early-type galaxies. Early-type galaxies are known to obey a strong correlation between velocity dispersion, effective radius, and magnitude known as the fundamental plane (Djorgovski & Davis 1987; Dressler et al. 1987), and we can estimate whether the lens galaxy as constrained by the lens models can lie on the fundamental plane. Kochanek

(1993, 1996), Breimer & Sanders (1993), and Grogin & Narayan (1996) have previously explored using stellar dynamical models as an added check on lens models.

For our comparison sample we adopted the data of Jørgensen, Franx & Kjørgaard (1995a,b, hereafter JFK). Figure 7 shows the JFK sample in the space of $\log \sigma$ and $\log r_e$ shifted to the redshift of PG 1115+080. The velocity dispersion σ was estimated for a fixed metric aperture of $3''.4$ in diameter at Coma (corresponding to $0''.4$ at PG 1115+080 for $\Omega_0 = 1$). In order to compare the K93 and JFK photometry, we converted the JFK Gunn r magnitudes to the K93 F785LP band by using the galaxy evolution models of Bruzual & Charlot (1993) to compute the K and evolutionary corrections and the $r - \text{F785LP}$ color (see Keeton et al. 1997b for details). We assumed that the luminosity density can be modeled by a Hernquist (1990) distribution with Hernquist scale length $a = 0.45r_e$, and we calculated only isotropic stellar dynamical models. From the models in §4.2, we know that with an SIS group the mass inside the ring of images (radius $r_0 = 1''.14 = 3.16h^{-1}$ kpc) is $1.22 \times 10^{11}h^{-1} M_\odot$, with a 5% uncertainty due to the position of the group, a 10% uncertainty (upwards) due to making the group more centrally concentrated, and a 7% uncertainty (upwards) due to the cosmological model.

Figure 7 superimposes the predicted PG 1115+080 aperture velocity dispersion as a function of effective radius on the JFK sample. The self-gravitating Hernquist (constant M/L) models have diverging central velocity dispersions for small effective radii because the mass is fixed by the lens model, forcing $\sigma \propto r_e^{-1/2}$ for effective radii smaller than the ring defined by the images. The effective radius is restricted to the rough range $1''.0 \lesssim r_e \lesssim 4''.0$ if the galaxy is to lie on the fundamental plane; then from §4.1 the de Vaucouleurs models with fixed group give $0.5 \lesssim h_{BC} \lesssim 0.7$ with an SIS group and $0.6 \lesssim h_{BC} \lesssim 0.9$ with a point mass group. Surprisingly, the dark matter models tend to have dispersion estimates that move along the fundamental plane. Nonetheless, many of the centrally-concentrated lens models that lead to high values for H_0 require a galaxy off the fundamental plane; for example, the $\alpha = -1$ model with $s = 0''.1$ that produces $h_{BC} = 0.77$ lies to the right of the JFK sample. These fundamental plane constraints can be made quantitative once we know the lens galaxy structure and effective radius.

Note that the Hernquist models require a total lens galaxy magnitude of $I(\text{F785LP}) \simeq 17$ in order to lie on the fundamental plane, whereas K93 estimated a central aperture magnitude for the lens galaxy of $I(\text{F785LP}) = 18.36$ mag. We experimented with the K93 images and found that, due to the wings of the original WFPC point-spread function and to the huge contrast between the quasar and galaxy surface brightnesses, the data are consistent with lens models having $I(\text{F785LP}) \simeq 17$ and $r_e \simeq 1''.5\text{--}2''.0$. In addition, Keeton et al. (1997b) have remarked that the K93 magnitude estimate gives a luminosity well below

that expected from the “Faber–Jackson” type relation between image separation and lens luminosity that other lenses obey. A higher luminosity for the PG 1115+080 lens galaxy would move it closer to the trend followed by other lenses. Improved HST photometry will reveal whether this is indeed the case.

Although this analysis is limited at present by the lack of optical data on the lens galaxy, it does reveal that the centrally-concentrated galaxy models that give high values for H_0 are physically implausible. The dark matter models are consistent with stellar dynamics, as are the constant M/L models if the effective radius is in the range $1''.0 \lesssim r_e \lesssim 4''.0$.

6. Discussion

By combining a lens model of PG 1115+080 with the observed time delays of Bar-Kana (1997), we can infer a value for H_0 that is independent of the standard distance ladder. The resulting value depends on the lens model, so we explored a range of models to understand the systematic uncertainties in the models, their effects on H_0 , and the types of future observations that can reduce the uncertainties. We found that PG 1115+080 cannot be fit by an isolated lens galaxy, but that it can be well fit ($\chi^2/N_{dof} < 1$) by including the effects of the nearby group. To understand the full range of model uncertainties, it is important to use an ellipsoidal galaxy and a movable group. Since the present observational data do not constrain the galaxy and group profiles or the group position, we studied various profiles and group positions and found good fits with H_0 ranging from roughly 30 to 90 $\text{km s}^{-1} \text{Mpc}^{-1}$. However, many of these models are unacceptable on physical grounds. For example, some of the models that give high values for H_0 require a galaxy mass profile that is more centrally concentrated than typical luminosity profiles and correspond to a galaxy that does not lie on the fundamental plane. If we restrict the models to a plausible constant M/L model and a dark matter model, we can use a Bayesian analysis to characterize the systematic uncertainties in H_0 relating to degeneracies in the models. We find $H_0 = 51_{-13}^{+14} \text{ km s}^{-1} \text{Mpc}^{-1}$, where the error bars incorporate the uncertainty in the measured time delays as well as the uncertainties in the lens models due to the group position and the galaxy and group profiles. They do not, however, take into account the systematic uncertainties in the value of the time delay ratio r_{ABC} from Bar-Kana (1997). In addition to the formal uncertainties, there may be a 5–10% uncertainty due to mass fluctuations from large-scale structure (Bar-Kana 1996; Wambsganss et al. 1997), and a 7% uncertainty (upwards) due to the cosmological model (Table 1).

The uncertainties in H_0 can be reduced with better observational constraints, but perhaps surprisingly not with better relative quasar positions and fluxes. In most models

the quasar positions are already overfit, and an order of magnitude improvement in the uncertainties (to 0.5 mas) is not practical. The quasar fluxes, by contrast, are dominated by systematic effects from microlensing and extinction rather than by measurement errors. We accounted for these effects by using flux error bars of 20%; merely reducing the flux error bars by a factor of two changes the absolute χ^2 but has little effect on the best-fit model parameters. Improving the constraints from the quasar fluxes would require understanding the systematic effects of microlensing and extinction, and in particular understanding why the K93 value of the A_2/A_1 flux ratio (0.66 in V and 0.70 in I) differs from the best-fit models (typically $\gtrsim 0.90$) and from theoretical expectations of a value near unity. One way to avoid problems with microlensing and extinction would be to measure radio flux ratios; unfortunately PG 1115+080 is not a strong radio source (flux < 1.5 mJy; Weymann et al. 1980).

The most promise for improving the constraints comes from the galaxy position and the time delays (see §4.2). Reducing the error bars on the galaxy position from 50 mas to 10 mas or better will rule out many models, and such a reduction should be possible with new WFPC2 observations. Reducing the error bars on the time delays by a factor of four (to ~ 0.5 day in the time delays or to ~ 0.05 in r_{ABC}) will provide a useful independent constraint. In fact, the time delay ratio r_{ABC} may provide the best probe of the galaxy profile. The effects of the galaxy position and the time delay ratio can be seen by noting that, together with the convergence at the ring of images, they account for almost all of the variation in H_0 from model to model. If we combine the models from §4.1 (different galaxy profiles with varying core radius and fixed group) and the models from §4.2 (singular isothermal ellipsoid or modified Hubble model galaxy, with movable group), then the implied Hubble constant is correlated with the galaxy position and the time delay ratio,

$$h_{BC} = \left[0.83 + 0.005\Delta x_{gal} - 0.006\Delta y_{gal} + 0.10(r_{ABC} - 1.4) \right] (1 - \kappa_0) \quad (9)$$

where Δx_{gal} and Δy_{gal} are the galaxy position in mas relative to that of K93, and $\kappa_0 = \kappa_{gal} + \kappa_{grp}$ is the total convergence at the ring of images due to the galaxy and the group. For a singular isothermal galaxy $\kappa_{gal} = 1/2$ at the ring of the images; for an SIS group $\kappa_{grp} = \gamma_{grp} \sim 10\%$ in PG 1115+080, while for a point mass group $\kappa_{grp} = 0$. This correlation is meant only as a qualitative guide to the quantities that will best constrain the Hubble constant, and it does not address the degree to which the convergence κ_0 can be determined from improved data.

If even with improved constraints we still cannot determine the galaxy and group profiles and the group position directly, then perhaps we can impose external considerations. First, as in §5 we can use stellar dynamics and the fundamental plane to identify which models are physically plausible. At present this analysis can only rule out very

concentrated models, but with luminosity profile data for the galaxy it may provide a more quantitative constraint. Unfortunately, directly measuring the central velocity dispersion in PG 1115+080 will be very difficult due to the high quasar/galaxy contrast. Second, we could require consistency with other gravitational lens statistics and models (Grogin & Narayan 1996; Kassiola & Kovner 1993; Kochanek 1993, 1995, 1996, Wallington & Narayan 1993; Maoz & Rix 1993) and with observations of elliptical galaxies (Fabbiano 1989; Rix 1996) to say that lens galaxies have significant dark matter and small core radii. In this case, the models from §4.2 give $H_0 = 44 \pm 11 \text{ km s}^{-1} \text{ Mpc}^{-1}$ using the r_{ABC} constraint. Finally, there are now two lenses (0957+561 and PG 1115+080) for which time delays have been measured. Both systems exhibit a degeneracy between the mass distribution and the Hubble constant (e.g. Grogin & Narayan 1996), but by requiring the lenses to agree on both the Hubble constant and the typical mass distributions of galaxies we may be able to break the degeneracies.

Acknowledgments: We thank P. Schechter, R. Bar-Kana, E. Falco, J. Lehár, R. Narayan, B. McLeod, M. Franx, and M. Geller for useful discussions. CRK is supported by ONR-NDSEG grant N00014-93-I-0774. CSK is supported by NSF grant AST-9401722.

REFERENCES

- Angonin-Willaime, M.-C., Hammer, F., & Rigaut, F., 1993, in *Gravitational Lenses in the Universe*, ed. J. Surdej, D. Fraipont-Caro, E. Gosset, S. Refsdal, & M. Remy (Liège: Institut d’Astrophysique), 85
- Bar-Kana, R., 1996, *ApJ*, 468, 17
- Bar-Kana, R., 1997, preprint astro-ph/9701068
- Bernstein, G.M., Tyson, J.A., & Kochanek, C.S., 1993, *AJ*, 105, 816
- Binney, J., & Tremaine S., 1987, *Galactic Dynamics* (Princeton: Princeton University Press)
- Bolte, M., & Hogan, C.J., 1995, *Nature*, 376, 399
- Borgeest, U., & Refsdal, S., 1984, *A&A*, 141, 318
- Breimer, T.G., & Sanders, R.H., 1993, *A&A*, 274, 96
- Bruzual A., G., & Charlot, S., 1993, *ApJ*, 405, 538

- Djorgovski, S., & Davis, M., 1987, ApJ, 313, 59
- Dressler, A., Lynden-Bell, D., Burstein, D., Davies, R.L., Faber, S.M., Terlevich, R.J., Wegner, G., 1987, ApJ, 313, 42
- Fabbiano, G., 1989, ARA&A, 27, 87
- Falco, E.E., Gorenstein, M.V., & Shapiro, I.I., 1985, ApJ, 289, L1
- Falco, E.E., Gorenstein, M.V., & Shapiro, I.I., 1991, ApJ, 372, 364
- Falco, E.E., Shapiro, I.I., Moustakas, L.A., & Davis, M., 1997, preprint astro-ph/9702152
- Fischer, P., Bernstein, G., Rhee, G., & Tyson, J.A., 1997, AJ, 113, 521
- Freedman, W.L., Madore, B.F., & Kennicutt, R.C., 1996, to appear in *The Extragalactic Distance Scale*, ed. M. Livio & M. Donahue (Cambridge University Press)
- Gebhardt, K. et al., 1996, AJ, 112, 105
- Greenfield, P.E., Roberts, D.H., & Burke, B.F., 1985, ApJ, 293, 370
- Grogin, N.A., & Narayan, R., 1996, ApJ, 464, 92; erratum 1996, ApJ, 473, 570
- Guiderdoni, B., & Rocca-Volmerange, B., 1988, A&AS, 74, 185
- Henry, J.P., & Heasley, J.N., 1986, Nature, 321, 139
- Hernquist, L., 1990, ApJ, 356, 359
- Jørgensen, I., Franx, M., & Kjaergaard P., 1995a, MNRAS, 273, 1097 (JFK)
- Jørgensen, I., Franx, M., & Kjaergaard P., 1995b, MNRAS, 276, 1341 (JFK)
- Kassiola, A., & Kovner, I., 1993, ApJ, 417, 450
- Keeton, C.R., & Kochanek, C.S., 1996, in *Astrophysical Applications of Gravitational Lensing*, ed. C.S. Kochanek & J.N. Hewitt (Dordrecht: Kluwer), 419
- Keeton, C.R., Kochanek, C.S., & Seljak, U., 1997a, ApJ, 482, in press
- Keeton, C.R., Kochanek, C.S., & Falco, E.E., 1997b, in preparation
- Kochanek, C.S., 1991a, ApJ, 373, 354
- Kochanek, C.S., 1991b, ApJ, 382, 58

- Kochanek, C.S., 1993, ApJ, 419, 12
- Kochanek, C.S., 1995, ApJ, 445, 559
- Kochanek, C.S., 1996, in *Astrophysical Applications of Gravitational Lensing*, ed. C.S. Kochanek & J.N. Hewitt (Dordrecht: Kluwer), 7
- Kormann, R., Schneider, P., & Bartelmann, M., 1994, A&A, 284, 285
- Kormendy, J., & Djorgovski, S., 1989, ARA&A, 27, 235
- Kovner, I., 1987, ApJ, 318, L1; erratum 1987, ApJ, 323, L155
- Kristian, J. et al., 1993, AJ, 106, 1330 (K93)
- Kundić, T. et al., 1996, preprint astro-ph/9610162
- Lehár, J., Hewitt, J.N., Roberts, D.H., & Burke, B.F., 1992, ApJ, 384, 453
- Maoz, D., & Rix, H.-W., 1993, ApJ, 416, 425
- Narasimha, D., Subramanian, K., & Chitre, S.M., 1982, MNRAS, 200, 941
- Narasimha, D., Subramanian, K., & Chitre, S.M., 1984, MNRAS, 210, 79
- Narasimha, D., Subramanian, K., & Chitre, S.M., 1986, Nature, 321, 45
- Pelt, J., Kayser, R., Refsdal, S., & Schramm, T., 1996, A&A, 305, 97
- Press, W.H., Rybicki, G.B., & Hewitt, J.N., 1992a, ApJ, 385, 404
- Press, W.H., Rybicki, G.B., & Hewitt, J.N., 1992b, ApJ, 385, 416
- Press, W.H., Teukolsky, S.A., Vetterling, W.T., & Flannery, B.P., 1992, *Numerical Recipes in Fortran* (Cambridge University Press)
- Ramella, M., Pisani, A., & Geller, M.J., 1997, AJ, 113, 483
- Refsdal, S., 1964, MNRAS, 128, 307
- Riess, A.G., Press, W.H., & Kirshner, R.P., 1996, ApJ, 473, 88
- Rix, H.-W., 1991, *Ph.D. Thesis*, University of Arizona, University of Michigan Press
- Rix, H.-W., 1996, preprint astro-ph/9611040
- Schechter, P.L. et al., 1997, ApJ, 475, L85

- Schneider, P., Ehlers, J., & Falco, E.E., 1992, *Gravitational Lensing* (New York: Springer)
- Schild, R.E., & Thomson, D.J., 1995, *AJ*, 109, 1970
- Vanderreist, C., Gosset, E., Remy, M., & Swings, J.-P., 1992, in *Lect. Not. Phys.*,
Volume 406, *Gravitational Lenses: Proceedings of a Conference Held in Hamburg,
Germany, 9–13 September 1991*, ed. R. Kayser, T. Schramm, & L. Nieser (New
York: Springer-Verlag), 107
- de Vaucouleurs, G., 1948, *Ann. d'Ap*, 11, 247
- Wallington, S., & Narayan, R., 1993, *ApJ*, 403, 517
- Walsh, D., Carswell, R.F., & Weymann, R.J., 1979, *Nature*, 279, 381
- Wambsganss, J., & Paczyński, B, 1994, *AJ*, 108, 1156
- Wambsganss, J., Cen, R., Xu, G., & Ostriker, J.P., 1997, *ApJ*, 475, L81
- Weymann, R.J., Latham, D., Angel, F.R.P., Green, R.F., Liebert, J.W., Turnshek, D.A.,
Turnshek, D.E., & Tyson, J.A., 1980, *Nature*, 285, 641
- Young, P.J., Gunn, J.E., Kristian, J., & Oke, J.B., 1980, *ApJ*, 241, 507
- Young, P.J., Deverill, R.S., Gunn, J.E., Westphal, J.A., & Kristian, J., 1981, *ApJ*, 244, 723

Table 1. Cosmological scale factors

	$(\Omega_0, \lambda_0) =$	(1, 0)	(0.1, 0)	(0.4, 0.6)	(0.2, 0.8)
1''	$(h^{-1} \text{ kpc})$	2.771	2.968	3.080	3.219
$\frac{D_l D_s}{2r_H D_{ls}}$		0.139	0.149	0.145	0.145
$\frac{(1+z_l) D_l D_s}{c D_{ls}}$	$(h^{-1} \text{ days arcsec}^{-2})$	30.49	32.73	31.68	31.80
Σ_{cr}	$(10^{11} h^{-1} M_\odot \text{ arcsec}^{-2})$	0.326	0.350	0.339	0.340
Σ_{cr}	$(h \text{ g cm}^{-2})$	0.888	0.831	0.747	0.686

Note. — Quantities are computed for $z_s = 1.722$, $z_l = 0.304$. The first two cosmological models are FRW cosmologies with the specified Ω_0 . The last two cosmological models are flat cosmologies with $\Omega_0 + \lambda_0 = 1$.

Table 2. Observational data

	x (")	y (")	F555W (mag)	F785LP (mag)
A1	−1.294	−2.036	16.90	16.12
A2	−1.448	−1.582	17.35	16.51
B	0.362	−1.949	18.87	18.08
C	0.000	0.000	18.37	17.58
G	−0.355	−1.322		18.36

Note. — Data from HST WFPC observations by Kristian et al. (1993). x is approximately west, y is approximately north. The internal position uncertainties are 5 mas for the quasar images and 50 mas for the galaxy. Formally, the relative fluxes are uncertain by 1.5% in I (F785LP) and 3% in V (F555W), while the zero-point for magnitudes is uncertain by 0.3 mag. The positions and Gunn r magnitudes of the group galaxies are as follows (Young et al. 1981): G1= ($d_{grp} = 23''.5$, $\theta_{grp} = -118^\circ$, $r = 18.96$), G2= ($12''.0$, -95° , 20.04), G3= ($18''.9$, -131° , 20.53).

Table 3. Galaxy + fixed group models

Galaxy:		de Vaucouleurs	Isothermal	Modified Hubble	$\alpha = -1$
SIS Group	r_e or s (")	1.00	0.00	0.19	0.42
	h_{BC}	0.65	0.41	0.65	0.75
	r_{ABC}	1.40	1.35	1.40	1.44
	b/a	0.87	0.97	0.87	0.82
	Δ_{gal} (mas)	27.5	12.3	29.5	44.4
	χ_{pos}^2	0.04	0.01	0.06	0.53
	χ_{flux}^2	1.64	2.27	1.60	1.49
	χ^2	1.98	2.34	2.01	2.82
Point Mass Group	r_e or s (")	3.00	0.00	0.27	0.47
	h_{BC}	0.68	0.51	0.83	0.97
	r_{ABC}	1.40	1.36	1.43	1.47
	b/a	0.84	0.90	0.78	0.73
	Δ_{gal} (mas)	41.4	27.2	55.3	69.3
	χ_{pos}^2	0.07	0.03	0.35	2.19
	χ_{flux}^2	1.98	2.31	1.77	1.98
	χ^2	2.74	2.63	3.34	6.09

Note. — Results from the best-fit galaxy + fixed group models. The group position is fixed at the flux-weighted centroid of the four galaxies (C4 in Figure 1). The de Vaucouleurs models were computed only for discrete r_e spaced by 0".5. The softened power-law models were computed with s varying continuously. The χ_{pos}^2 and χ_{flux}^2 indicates the contribution to the χ^2 from the quasar positions and fluxes, respectively. Each model with fixed r_e or s has $N_{dof} = 5$. We do not give error bars because they would not encompass the effects of allowing the group to move.

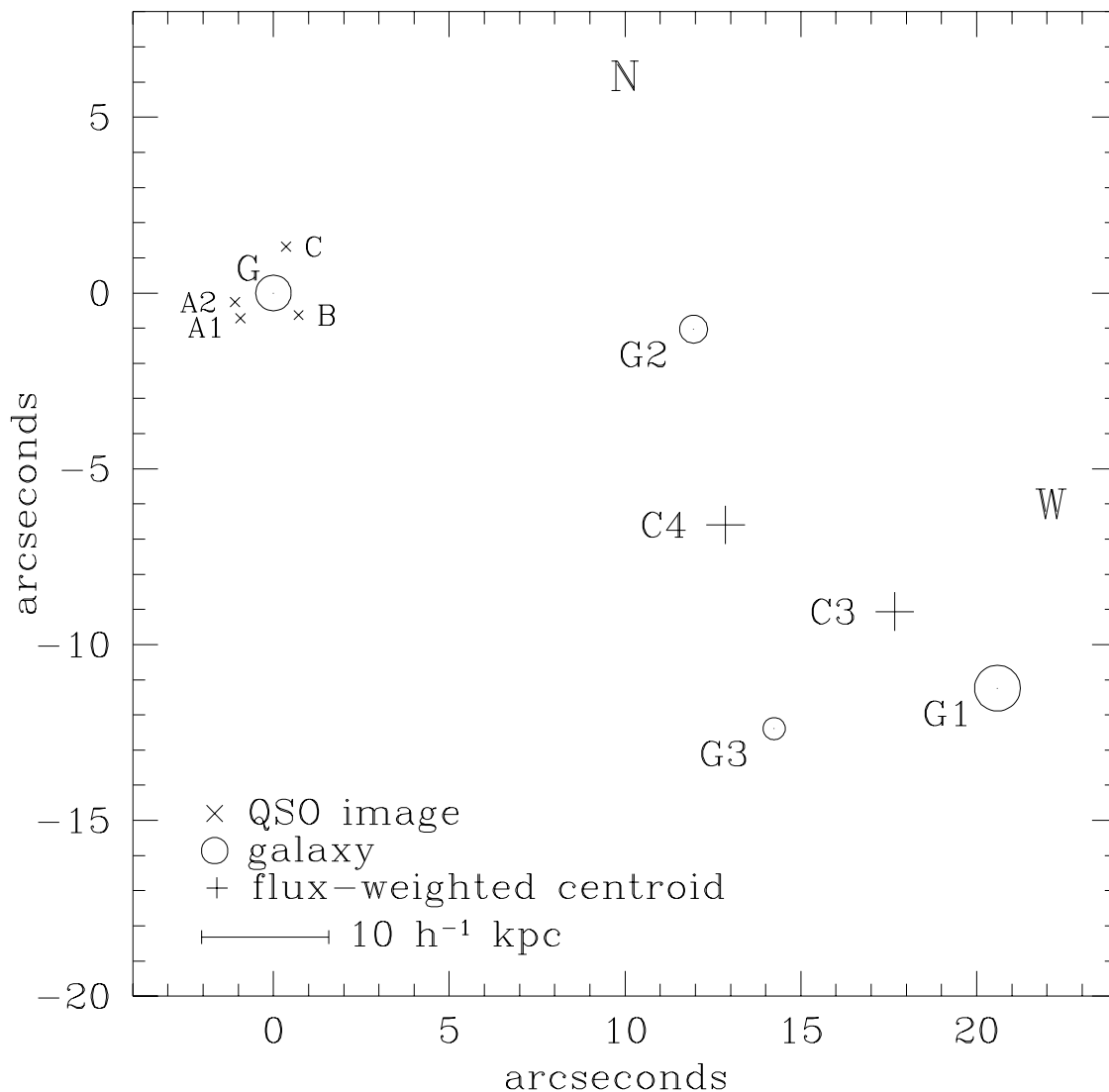


Fig. 1.— Schematic diagram of the gravitational lens PG 1115+080 and the nearby group. The crosses represent the four quasar images (K93). The circles represent the galaxies (Young et al. 1981), with the areas of the circles indicating the relative fluxes. The plusses represent (“C3”) the flux-weighted centroid of the three group galaxies and (“C4”) the flux-weighted centroid of all four galaxies. The physical scale indicated is for an $\Omega_0 = 1$ cosmology.

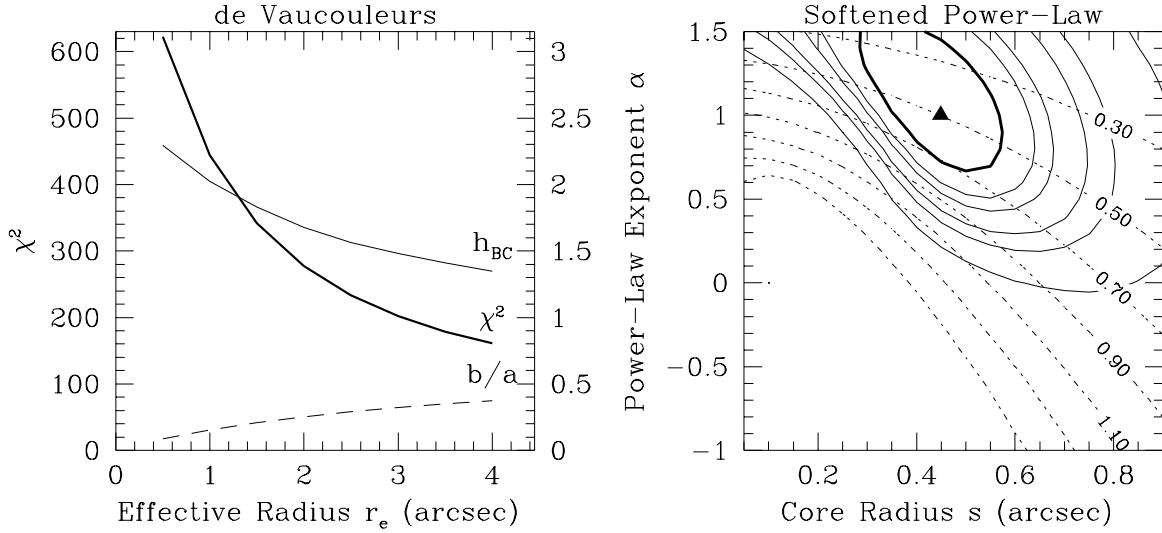


Fig. 2.— Results for models using only the primary lens galaxy. The galaxy is represented by an ellipsoidal mass distribution with the specified density profile. Each model with fixed r_e or (s, α) has $N_{dof} = 6$. *Left*: de Vaucouleurs profile. The heavy solid line is the χ^2 using the axis scale on the left. The light solid line is the Hubble constant expressed as $H_0 = 100h_{BC}(\Delta\tau_{BC}/25.0 \text{ days})^{-1} \text{ km s}^{-1} \text{ Mpc}^{-1}$, and the dashed line is the axis ratio of the galaxy; both use the axis scale on the right. *Right*: Softened power-law profile. The solid lines are contours of χ^2 drawn at $\Delta\chi^2 = 2.30, 4.61, 6.17, 9.21, 11.8,$ and 18.4 , the $1\sigma, 90\%, 2\sigma, 99\%, 3\sigma,$ and 99.99% confidence levels for two parameters. The dotted lines are contours of h_{BC} . The best-fit model (marked with a triangle) is at $s = 0''.449, \alpha = 1.002$ and has $\chi^2 = 46.9$ and $h_{BC} = 0.50$.

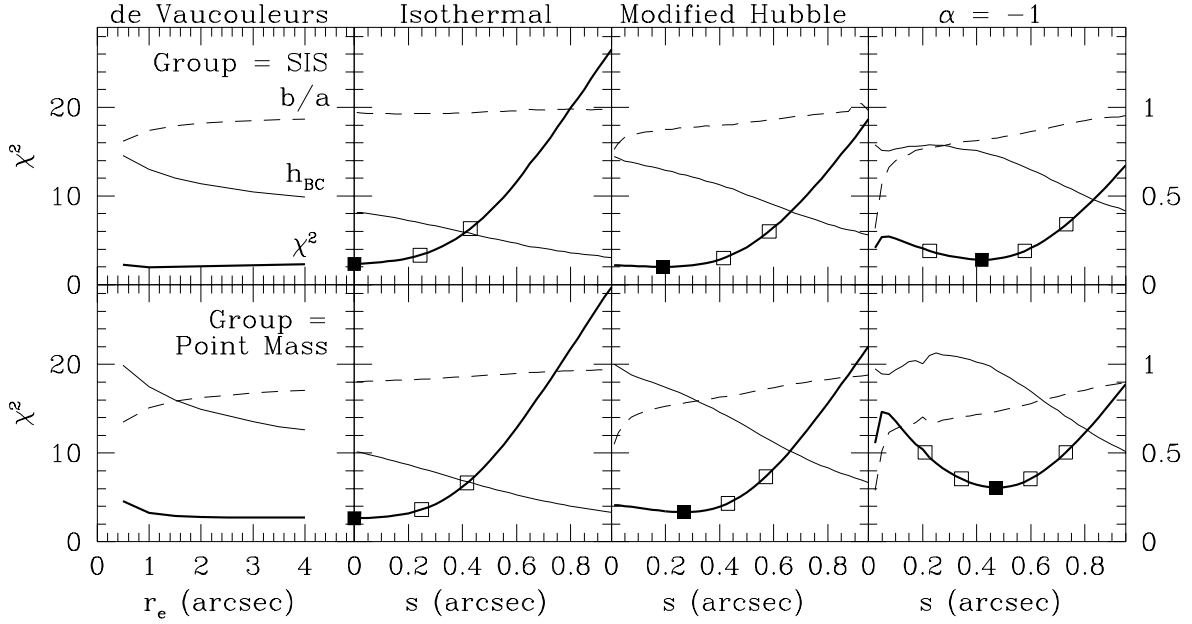


Fig. 3.— Results for models using the primary lens galaxy plus the nearby group. The group position is fixed at the flux-weighted average of the four galaxies (C4 in Figure 1). The primary lens galaxy is represented by an ellipsoidal mass distribution and the group is represented by a circular mass distribution. *Top*: the group is represented by an SIS. *Bottom*: the group is represented by a point mass. The heavy solid line is the χ^2 using the axis scale on the left; each model with fixed r_e or s has $N_{dof} = 5$. The filled and open points indicate the best fit and the $\Delta\chi^2 = 1$ and $\Delta\chi^2 = 4$ limits. The light solid line is h_{BC} and the dashed line is the axis ratio of the galaxy, both using the axis scale on the right.

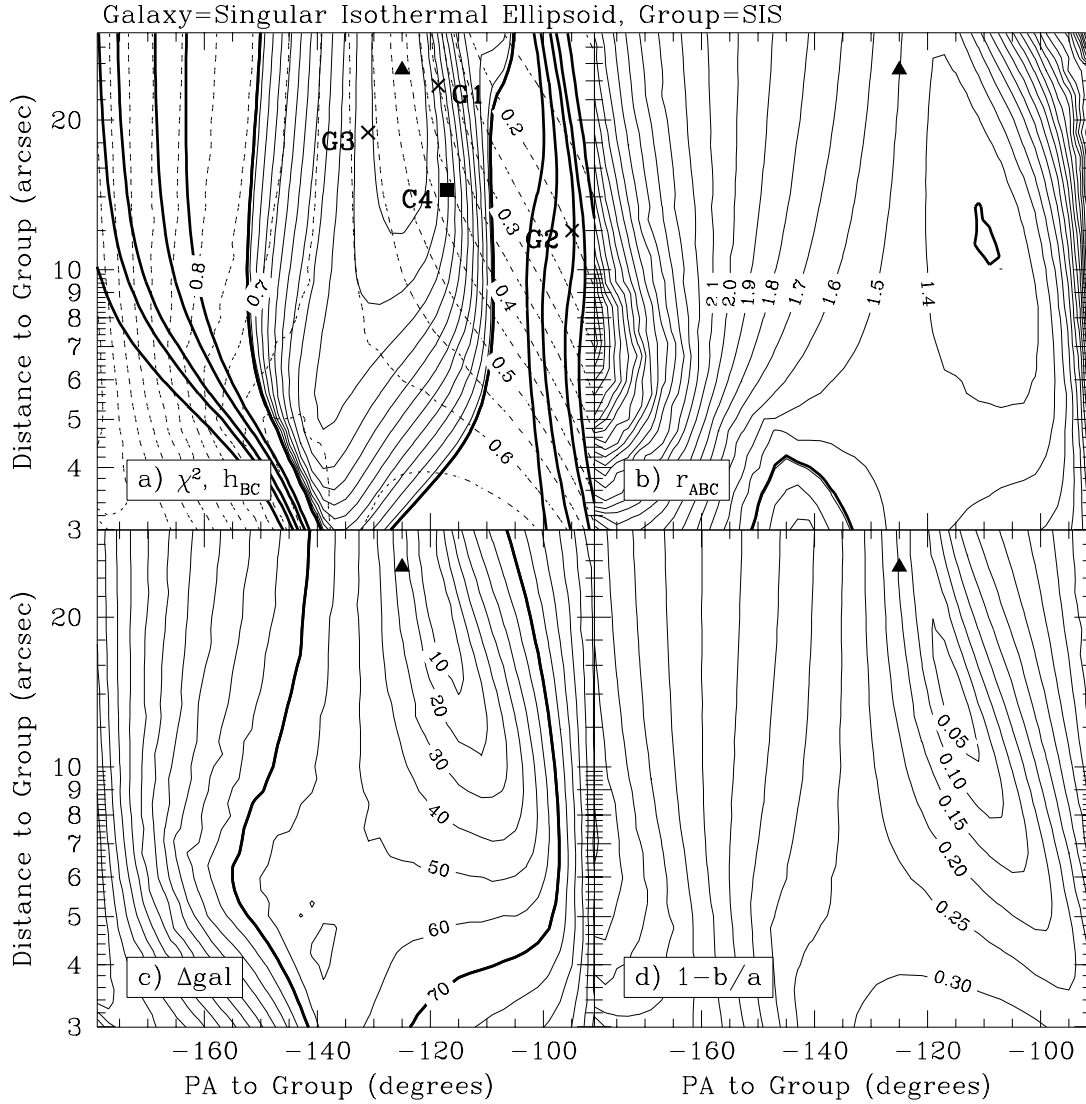


Fig. 4.— Results for models representing the primary lens galaxy as a singular isothermal ellipsoid and the group as an SIS. With the group position fixed a model has $N_{dof} = 5$. (a) The solid lines are contours of χ^2 drawn at $\Delta\chi^2 = 0.2, 0.4, \dots$ (light) and at $\Delta\chi^2 = 2.30, 4.61, 6.17, 9.21, 11.8, \text{ and } 18.4$ (heavy), the 1σ , 90%, 2σ , 99%, 3σ , and 99.99% confidence levels for two parameters. The dashed lines are contours of h_{BC} . The positions of the group galaxies and of the flux-weighted centroid (C4 in Figure 1) are indicated. (b) Contours of the time delay ratio r_{ABC} . The heavy contours indicate the 1σ range $1.13^{+0.18}_{-0.17}$ from Bar-Kana (1997). (c) Contours of the distance $\Delta_{gal} = |\vec{x}_{mod} - \vec{x}_{obs}|$ (in mas). The heavy contour indicates the range allowed by the Kristian et al. (1993) error bars, $\Delta_{gal} \leq \sqrt{2} \times 50$ mas. (d) Contours of the galaxy ellipticity $1 - b/a$. In the upper right corner the galaxy is oriented approximately North–South, and everywhere else it is approximately East–West. The best-fit model (marked with a triangle) is at $d_{grp} = 25''.2$ and $\theta_{grp} = -125^\circ$ and has $\chi^2 = 1.77$, $h_{BC} = 0.47$, $r_{ABC} = 1.50$, $\Delta_{gal} = 25$ mas, and $b/a = 0.85$.

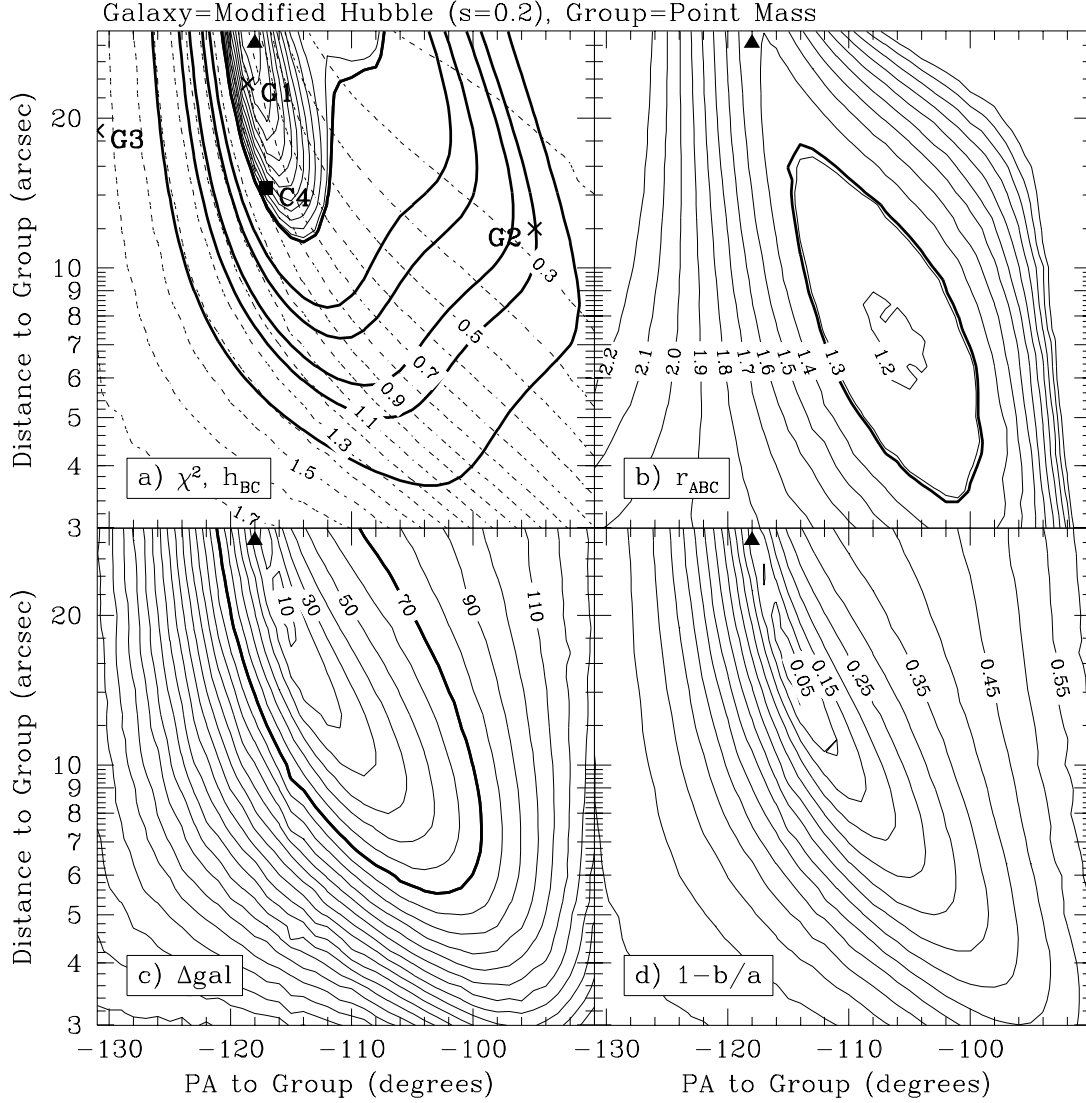


Fig. 5.— Results for models representing the primary lens galaxy as a modified Hubble model with core radius $s = 0.2$ ($0.55h^{-1}$ kpc) and the group as a point mass. The panels are the same as in Figure 4, except that the range of position angles is smaller. Again in (d) the galaxy is oriented approximately East–West in the lower left and North–South in the upper right. The best-fit model (marked with a triangle) is at $d_{grp} = 28.3$ and $\theta_{grp} = -118^\circ$ and has $\chi^2 = 1.70$, $h_{BC} = 0.67$, $r_{ABC} = 1.43$, $\Delta_{gal} = 16$ mas, and $b/a = 0.92$.

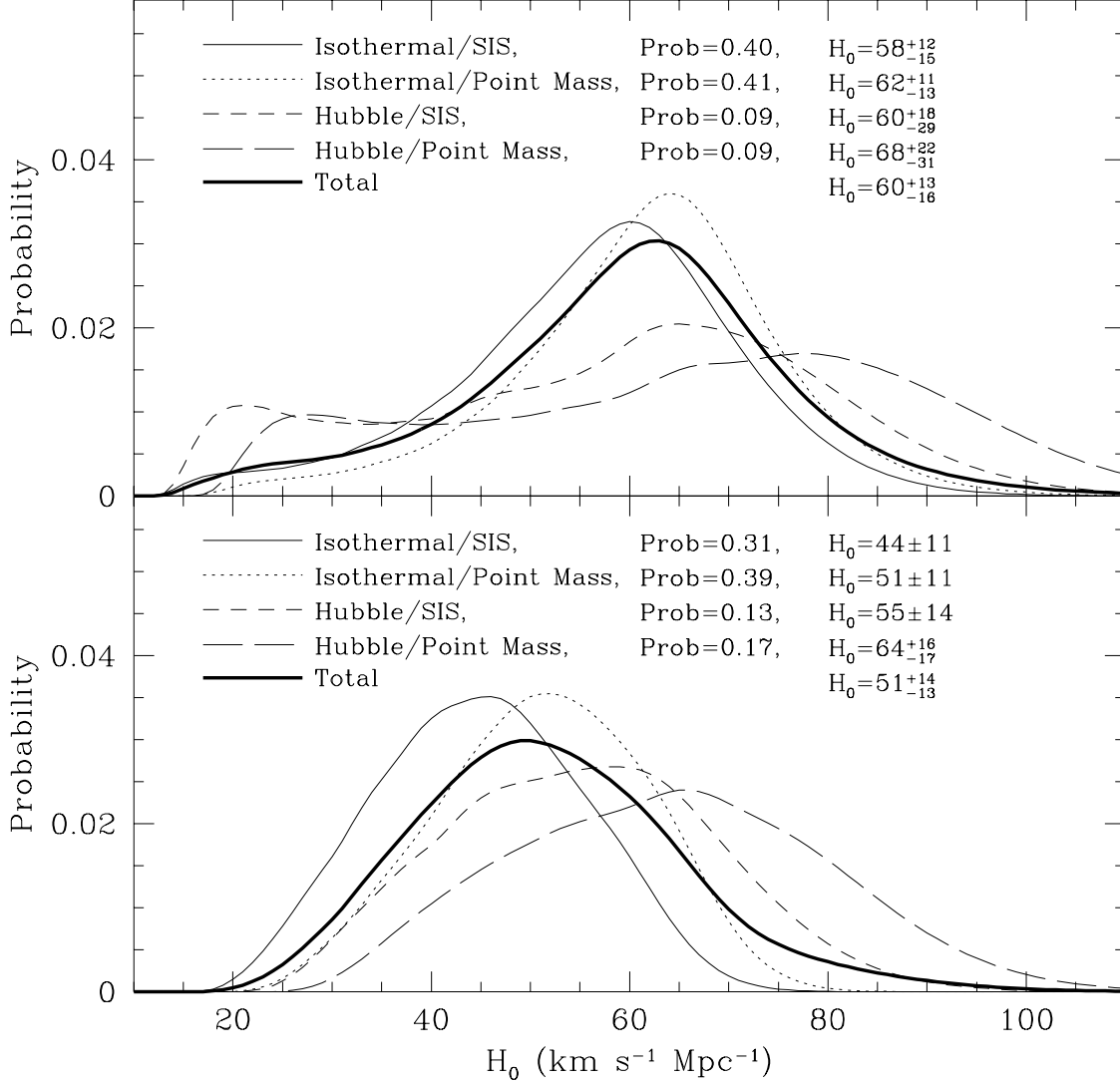


Fig. 6.— Normalized probability distributions for H_0 . The distributions were computed from a Bayesian analysis of the four classes of models discussed in §4.2. In the top panel the Bayesian analysis does not use the constraint from r_{ABC} , and in the bottom panel it does use r_{ABC} . The relative probabilities of the four models and their implied values for H_0 are given in the key. The spread within each distribution is due to the 6% uncertainty in the observed time delay and to the degeneracy in the group position. The spread between the distributions is due to the degeneracies in the profiles of the galaxy and the group.

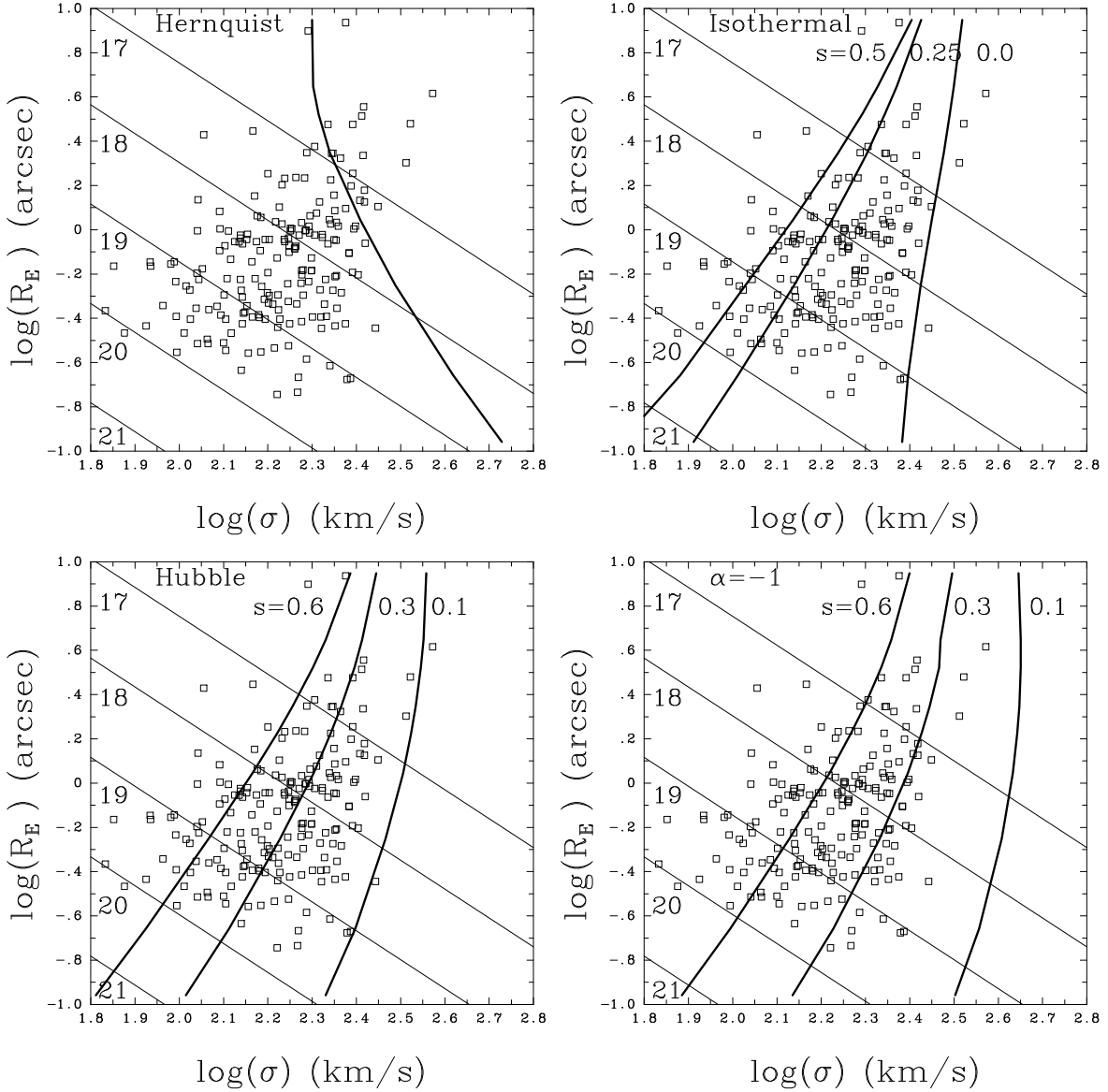


Fig. 7.— Stellar dynamical limits. The points show the effective radii and central dispersions of the JFK sample of cluster galaxies, with the effective radius rescaled to the redshift of PG 1115+080. The heavy solid lines show the central dispersion for the lens galaxy assuming the same metric aperture as a function of r_e ; for the softened power-law models, the core radius s is given in arcsec. The light solid lines show the F785LP magnitude estimates for the lens galaxy from the fundamental plane. The K93 value $I(\text{F785LP}) = 18.4$ is a central aperture magnitude and represents a lower bound. We found that the K93 images are consistent with a galaxy having $r_e \simeq 1''.5$ and $I(\text{F785LP}) \simeq 17$.